ORGANIZATION OF CONNEXONS IN ISOLATED RAT LIVER GAP JUNCTIONS

EDWARD GOGOL AND NIGEL UNWIN
Department of Cell Biology, Stanford University School of Medicine, Stanford, California 94305

ABSTRACT Gap junction plaques from rat liver plasma membranes have been subjected to a range of detergent treatments in order to evaluate systematically the influence of different isolation procedures on their structure. The separation of the connexons was found to vary depending on the conditions used. In the absence of detergent the center-to-center separation of the connexons is, on average, ~90 Å, and they are arranged on a hexagonal lattice so that the symmetry of the double-layered structure approximates to p6m in projection (or p622 in three-dimensions). Exposure to increasing concentration of detergent reduces the connexon separation to values below 80 Å. More severe detergent treatment leads to disintegration of the gap junction plaques. Specimens with center-to-center separations smaller than 86 Å show progressively larger deviation from p6m symmetry, seen as apparent rotations of the connexon assemblies within the crystal lattice. This reorganization occurs with both ice-embedded and negatively-stained specimens, using ionic or nonionic detergents, and therefore is probably a packing readjustment caused by depletion of intervening lipid molecules.

INTRODUCTION

Gap junctions are regions of contact between the plasma membranes of adjoining animal cells which are specialized to facilitate the passage of ions and small molecules between the cell interiors (for reviews, see references 11 and 15). They are composed of hexamers of a single polypeptide (M_r 28,000 [9, 7]), the amino acid sequence of which has recently been determined (14, 10). The hexamers, called connexons, protrude from the apposed membranes into the extracellular space and link up pairwise in register, forming a continuous cell-to-cell aqueous pathway. This communication channel appears to be involved in coordinating the metabolism (17) and differentiation (22) of connected cells, and in facilitating transmission of electrical signals (5).

Gap junctions have been isolated from the plasma membranes of hepatocytes for biochemical and structural investigation by virtue of their resistance to detergents (6, 7, 9, 23) and to harsh alkaline treatment (8). The isolated plaques consist of double membranes with the paired connexon assemblies often arranged in a regular way on a two-dimensional hexagonal lattice. However, it is unclear how the organization and conformation of these assemblies is affected by the various isolation protocols, and thus how their structure within an isolated gap junction relates to their structure in vivo. A large range in the average center-to-center separation of the connexons has been found in different preparations by x-ray diffraction (3, 12, 18) and electron microscopic images have shown variations in their arrangement. In the first low dose electron microscopy study (23), the hexagonal projection of the connexon assembly was observed to align approximately with the hexagonal unit cell vectors (p6m symmetry). Subsequent analyses noted a significant degree of apparent twisting of this assembly with respect to the unit cell vectors (p6 symmetry) (1, 7, 19). An understanding of the physical basis for these differences in apparent rotation (which has been termed skewing [1]) could lead to a rational basis for improving the structural order and hence obtaining information at higher resolution.

Here we evaluate the effect of variations in the isolation procedure on the organization and projected appearance of the connexon assembly. We show that the degree of skewing and the dimension of the crystal lattice are related to the severity of the detergent treatment. Based on the systematic differences seen with increasingly severe treatments, the best approximation to the *in vivo* structure of the gap junction seems to be one in which the connexon assembly is not strongly skewed but is organized in a lattice with approximate p6m symmetry (i.e., p622 symmetry in three-dimensions).

All correspondence should be sent to Dr. Gogol's present address at the Institute of Molecular Biology, University of Oregon, Eugene, OR 97403.

Dr. Unwin's present address is the MRC Laboratory of Molecular Biology, Hills Road, Cambridge CB2 2QH, England.

MATERIALS AND METHODS

Materials

Sodium deoxycholate and dodecyl maltoside were obtained from Calbiochem (La Jolla, California); n-lauryl sarcosine (Sarkosyl NL-97) was

from ICN Pharmaceuticals, Inc., Irvine, CA. All other chemicals were of reagent grade and obtained from standard sources. Rats used were small Sprague-Dawley males (160–200 g body weight).

Specimen Preparation

Plasma membranes were prepared from freshly excised rat livers and purified on sucrose gradients after a previously published procedure (23). In some cases, membranes were isolated using an aqueous two-phase polymer system (13). In both cases the protease inhibitor phenyl methyl sulfonyl fluoride was added to a concentration of 0.5 mM at each stage of the preparation. After their final pelleting, the membranes were resuspended in dilute bicarbonate buffer (5 to 20 mM) at pH 7.5 to 8.0, with 0.05% sodium azide present.

In order to study detergent-dependent changes in connexon organization, the plasma membranes were exposed to a series of concentrations of sodium deoxycholate or Sarkosyl. The membranes were dialyzed against a 100-fold or larger volume of bicarbonate buffer (10 to 20 mM, pH 7.5 to 8.2) containing detergent concentrations spanning the range 0 to 2%. Samples were loaded into fast-dialyzing tubing (Spectra/Por 2, Spectrum Medical, Los Angeles, CA) and dialyzed for 20 h at 5°C (deoxycholate) or for 8 h at room temperature (Sarkosyl). This dialysis procedure ensured that the ratio of protein to free detergent would be unaffected by variations in lipid content between the different plasma membrane preparations. The dialysates were pelleted (25,000 rpm for 20 min., [Ti50 rotor; Beckman Instruments, Palo Alto, CA]), washed, and resuspended in buffer. The samples were disaggregated by sonication for ~10 s with a micro-ultrasonic cell disruptor (Kontes, Vineland, NJ) set at full power output. The preparations were used without any further attempt at purification.

Preparations were also made by sonicating plasma membranes in alkaline conditions (8), a method which yields purified junctions while avoiding the use of detergents. SDS gel analysis showed that these preparations contained a major band of 28,000 M_r, along with a dimeric form with an M_r of 54,000. Contaminants were visible only in very minor amounts, although material not entering the gel was also present. These specimens were examined directly, or exposed to low (0.005 to 0.1%) concentrations of the nonionic detergent dodecyl maltoside, with no change in the SDS gel patterns. Manipulations were carried out at 0–4°C.

Electron Microscopy and Image Processing

Negatively stained samples were prepared by pelleting small volumes (~25 μl) of a dilute suspension at ~1,000 g for 3–5 min onto glow-discharged carbon-coated grids. The grids were briefly washed with water, floated on a drop of 2% uranyl acetate, wicked to remove excess stain, and dried at room temperature. Samples for cryoelectron microscopy were similarly applied, washed with water, blotted and plunged into liquid ethane cooled with liquid nitrogen to just above its freezing point. The frozen grids were stored under liquid nitrogen.

Samples were examined at 100 KV with an EM400 electron microscope, (Philips Electronic Instruments, Mahwah, NJ) equipped with a low-dose kit and an additional anticontaminating device for low temperature work. Grids of negatively stained samples were inserted into the microscope with the specimen side down. Grids of frozen samples were mounted in a liquid nitrogen cooled holder (Gatan, Inc., Warrendale, PA). Images were recorded on Kodak SO163 film at a total dose of 5–10 electrons/Å^2. The microscope magnification was calibrated on a daily basis by photographing catalase crystals or calibration grids (Ted Pella, Tustin, CA) at the lens currents used for recording micrographs. Measured values of the magnification ranged from 36,000 to 39,000X.

Images were initially examined visually, and discarded if the junctions did not show an excess of stain or ice at their edges, since incomplete embedding may lead to serious misrepresentation of the true projected structure (21). They were then studied by optical diffraction, and areas were selected on the basis of the sharpness, resolution, and hexagonal symmetry of the diffraction peaks. All image areas chosen for processing had optical diffraction patterns extending to at least the (2, 1) reflection, and often further (Fig. 1 *a*, insets). Selected areas of the micrographs were digitized with a flatbed microdensitometer (Perkin-Elmer Corp., Physical Electronics Div., Eden Prairie, MN) at a spot and step size of 25 μm (equivalent to a sampling of 6.5 Å at the specimen). The numerical arrays were Fourier transformed and amplitude peaks were fitted iteratively to a lattice. Unit cell dimensions were derived from the reciprocal lattice vectors, and those images having unit cell parameters differing by more than 3% from the ideal values ($\gamma = 60°$, $a = b$) were not used.

Amplitudes and phases were extracted from transform values at the reciprocal lattice points (Table I), and always extended reliably (amplitudes minimally 50% above background) to a resolution of at least 25 Å. More strongly diffracting images were processed to higher resolution, up to the fourth order (~17 Å). Data sets were refined to p6 symmetry, and only those with low phase errors (unweighted root mean square errors of <15° in negative stain and 20° in ice) were used in synthesizing the projection maps. The amplitudes of reflections at resolutions >25 Å were weak compared with the amplitudes of the low-resolution reflections, and the corresponding phases usually refined to real values poorly. Addition of these reflections had no significant effect on the projection maps.

The apparent rotation of the connexon assembly within the crystal lattice (i.e., the skew angle) was measured from the projection maps by noting the angular position of either of two sets of approximate mirror planes. One of these mirror planes connects the density peaks on opposite sides of the connexon assembly (solid lines, Fig. 2 A and B), and the other is 30° away, lying between the peaks (Fig. 2 C and D). The skew angle was defined by the minimum angle made by either of these planes with the unit cell vectors, thus allowing a range of 0° to 15° in either a clockwise or counterclockwise direction. (For p6m symmetry, one of the axes would be aligned exactly with a unit cell vector, giving a skew angle of 0°.)

The hand of an image was defined by the direction of the skew angle, clockwise regarded as right-handed. Of the 54 images of negatively stained specimens with a clearly measurable skew angle (>3°), 34 were right-handed. While this distribution is asymmetric, it is within an acceptable range of scatter (<2 SD from the mean of a normal distribution) for an equal probability of both hands. A similar distribution and conclusion has been reported previously (1, 2). Since we found no systematic difference between images of opposite hand, all left-handed images were flipped (by exchanging the *h* and *k* indices) for quantitative analysis and comparison.

Variations in strength of the six-fold modulations present in individual images were evaluated by calculating rotational power spectra (4) from projection maps, to a radius of 30 Å around the channel. The six-fold terms were normalized to their respective radial (zero-order) terms to obtain a measure of the modulation.

RESULTS

Gap junctions in plasma membrane preparation were enriched, and also altered in their morphology, by increased exposure to detergent. With low detergent concentrations curved and partially vesiculated junctions were most frequent, whereas at higher detergent concentrations junctions were present mainly as flat sheets. At the highest concentrations, holes and cracks appeared more frequently in the plaques, limiting the potential extent of crystalline domains.

The appearance of the junctions in low and high detergent preparations is shown in Fig. 1. Over the range of concentration used, detergent did not cause gross changes in the projected structure of the individual connexon assemblies, whether embedded in stain (Fig. 1 *A* and *B*) or in ice (Fig. 1 *C* and *D*). However, their center-to-center

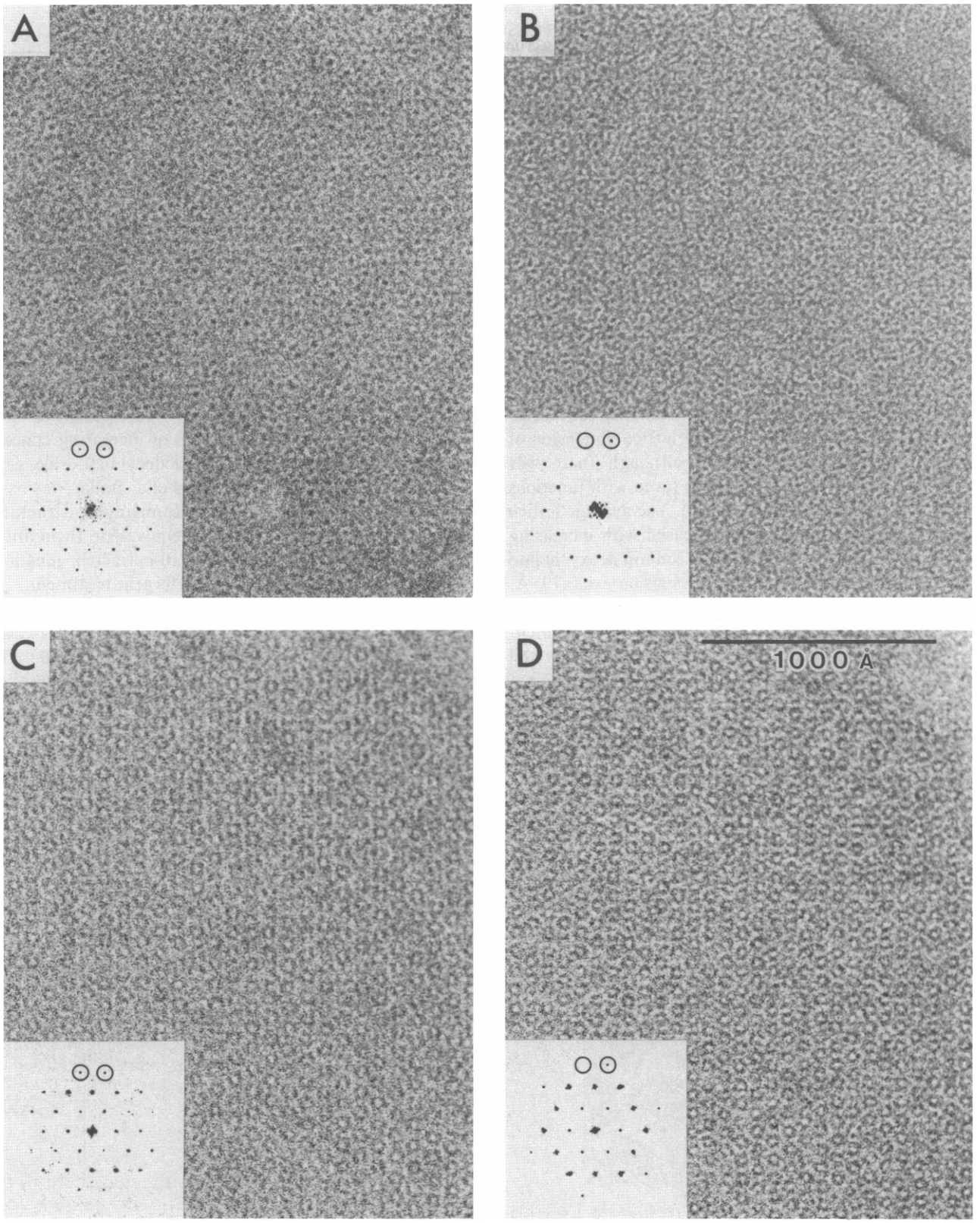

FIGURE 1 Low-dose electron micrographs of uranyl acetate stained (*a* and *b*) and ice-embedded (*c* and *d*) gap junctions. Samples in *a* and *c* have not been exposed to any detergents (plasma membrane and alkaline preparations, respectively), and have large lattice dimensions (~90 Å); those in *b* and *d* have been exposed to detergent (0.5% Sarkosyl and 0.1% dodecyl maltoside, respectively), and have small lattices (~82 Å). The insets are computed diffraction patterns typical of each specimen. In *a* and *c*, the (1, 2) and (2, 1) reflections (*circled*) are of similar strength; in *b* and *d* they are unequal.

TABLE I
AMPLITUDES AND PHASES OF AVERAGED DATASETS

	Stain				Ice			
No. Images	13		12		5		7	
d (SD)*	90.0 (0.9) Å		81.4 (0.7) Å		88.1 (1.2) Å		80.8 (0.8) Å	
Phase Error‡	9.0°		13.0°		10.6°		12.7°	
h, k	Amp(SD)	Phase	Amp(SD)	Phase	Amp(SD)	Phase	Amp(SD)	Phase
1,0	211(116)	0	84(32)	0	199(52)	180	94(58)	180
1,1	284(44)	180	378(32)	180	298(47)	0	396(25)	0
2,0	327(24)	180	310(18)	180	398(22)	0	393(21)	0
1,2	177(28)	180	80(21)	180	131(38)	0	100(38)	180
2,1	209(32)	180	231(25)	180	173(30)	0	109(18)	0
3,0	11(28)	180	18(32)	0	41(35)	0	0(0)	0

*Average values and standard deviations of the lattice dimensions.
‡Average unweighted deviations from 0 or 180°, for all nonzero reflections to the third order.

separation was noticeably smaller at the higher concentrations (Fig. 1 *B* and *D*). The average lattice dimension of untreated membranes was 89 Å, although there was considerable scatter about this figure (even with junctions from a single membrane preparation). The average lattice dimension and also the scatter decreased with increasing concentrations of the ionic detergent, sodium deoxycholate (Fig. 3). The minimum lattice dimension was 79 Å. Similar results were obtained with another ionic detergent, Sarkosyl (data not shown). No difference in lattice dimensions was found between specimens preserved in stain and in ice.

Junctions prepared by alkali extraction of plasma membranes usually contained much smaller crystalline domains than junctions in untreated or detergent-treated membranes, and yielded strong diffraction (i.e., to a resolution of 25 Å) less frequently. Lattice dimensions measured from ordered areas of these junctions were similar to those of untreated membranes. Addition of increasing concentrations of the nonionic detergent, dodecyl maltoside, gave rise to progressively smaller lattices in a similar way as in Fig. 3 (data not shown). The accompanying structural effects (described below) were also equivalent. In addition, well-ordered domains in the alkali-extracted junctions became more abundant after the detergent treatment.

Projection maps from negatively stained junctions showed a systematic variation of skew angle (see Materials and Methods) with lattice dimension (Fig. 2 *A* and *B*). The observed range of angles was 0–12.5°, and the distribution of skew angles was similar for left- and right-handed images. Fig. 4 plots the dependence of skew angle on lattice dimension. The skew angle increases as the lattice contracts (left to right in these plots). It is close to 0°, taking into account the errors involved (we estimate the error in measurement as 2° to 5°, depending on the image), down to

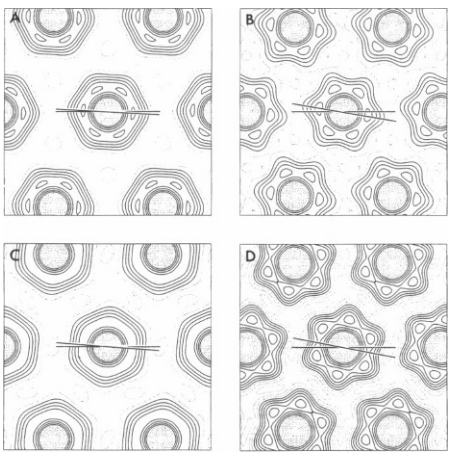

FIGURE 2 Projection maps calculated from the averaged datasets in Table I. *a, b*: stained junctions with lattice dimensions of 90 and 81 Å, respectively. *c, d*: ice-embedded junctions with lattice dimensions of 88 and 81 Å, respectively. Two lines are drawn on each map to indicate the apparent rotation, or skew, of the connexon assembly with respect to the unit cell axes. The skew angles estimated from these four maps are *a*: 3°, *b*: 12°, *c*: 4°, *d*: 14°.

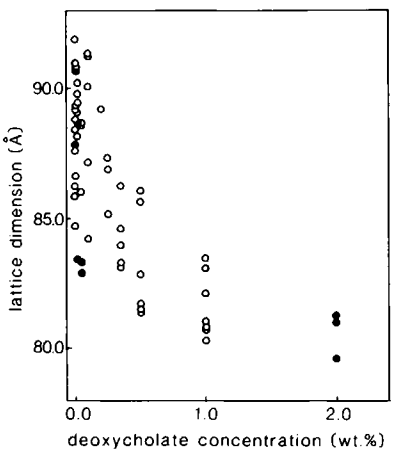

FIGURE 3 Lattice dimension decreases with increasing concentration of detergent. Dimensions measured from 61 images are plotted against the concentration of deoxycholate to which each sample was exposed. Open and filled circles indicate data from stained and ice-embedded junctions, respectively.

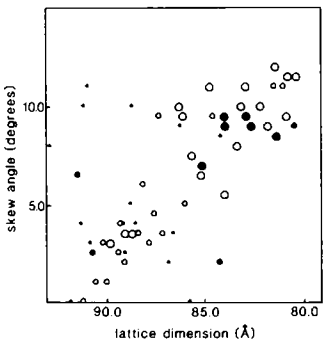

FIGURE 4 Skew angles increase as the lattice becomes smaller. The skew angles are plotted against the lattice dimensions determined from images of stained junctions. The symbol sizes are proportional to the values of the six-fold terms from rotational analysis of each image, and reflect the reliability with which each angle has been measured. Closed and open circles correspond to Sarkosyl and deoxycholate treated specimens, respectively.

a lattice dimension of ~86 Å, but becomes significant for all junctions with lattice dimensions below this value.

Projection maps of ice-embedded junctions showed similar changes in skew angles with lattice dimension (Fig. 2 *C* and *D*), although the density peaks around the connexon assembly were in different positions (30° away from those in the negative stain maps). The skew angles for ice-embedded junctions having large lattice dimensions were also more variable than those of similar negatively stained specimens.

The degree and direction of skewing in projection maps is correlated with the relative strengths of the (1, 2) and (2, 1) reflections (see Fig. 1, insets). The ratio of these measurements was calculated for each image (Fig. 5). With the stained junctions (Fig. 5 *A*), the ratio (1, 2):(2, 1) dropped monotonically as the lattice became smaller. Significant deviations from unity were usually observed with junctions having lattice dimensions of ~86 Å or less. With the ice-embedded junctions a similar but more dramatic relationship was observed (Fig. 5 *B*),

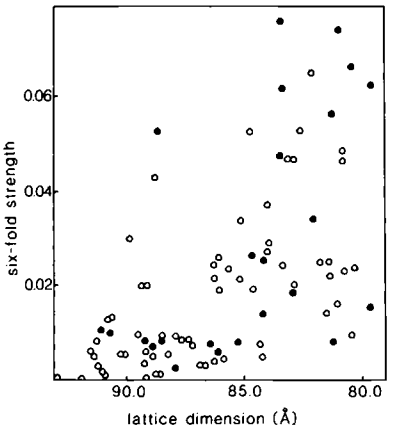

FIGURE 6 The six-fold modulation of the connexon assembly increases as the lattice becomes smaller. The values of the six-fold rotational terms of individual images (normalized to the zero-order or radial term of each image) are plotted against the measured lattice dimensions. *Open circles:* stained junctions; *filled circles:* ice-embedded junctions.

including a reversal of the phase of the (2, 1) reflection as the lattice became smaller (Table I). Only a few of these images, with large lattice dimensions, had ratios differing insignificantly from one.

The six-fold modulations created by the connexons also changed with change in lattice, becoming stronger as the connexons came closer together. This effect is evident in maps of stained (Fig. 2 *A* and *B*) and, more markedly, ice-embedded specimens (Fig. 2 *C* and *D*), and is plotted in Fig. 6.

DISCUSSION

Most conventional methods of isolating gap junctions rely on their resistance, relative to the remainder of the plasma

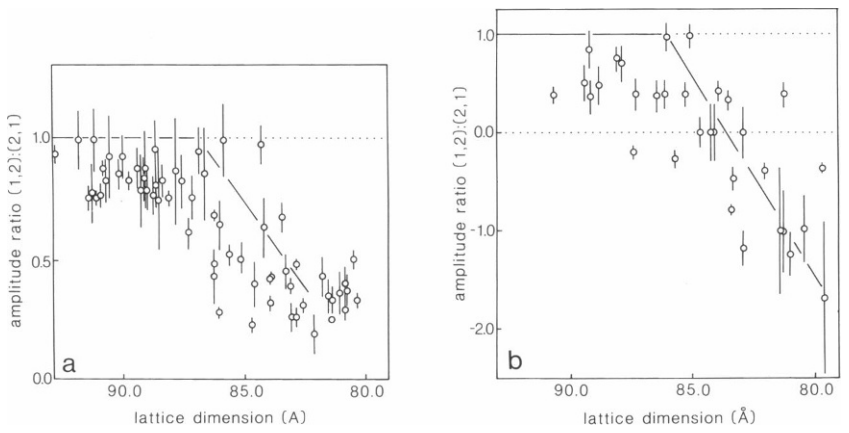

FIGURE 5 The amplitude ratio of the (1, 2):(2, 1) reflections decreases as the lattice becomes smaller, producing a systematic deviation from p6m projection symmetry: *a*, stained; and *b*, ice-embedded specimens. The data include untreated, detergent-extracted plasma membranes and alkali-extracted gap junctions. Error bars equal to +/− 1 SD are drawn for each point. The standard deviation was estimated from the variation in amplitude among the three measurements related by p6 symmetry for each reflection. The dotted horizontal line indicates the ratio of unity corresponding to p6m symmetry, and the broken solid line depicts our interpretation of the overall trend relating the (1, 2):(2, 1) ratio to lattice dimension (see text). The relationship is more sensitive with the ice-embedded junctions, as the line has a much steeper slope, and crosses from positive (*same phases*) to negative (*opposite phases*) values for the (1, 2):(2, 1).

membrane, to disruption by detergents. The effects of these treatments on the resulting specimens have not been systematically explored, although changes in the x-ray scattering pattern with different isolation protocols have been noted (3, 12, 17). Here we report on progressive changes in connexon packing and projection structure induced by exposure to increasing concentrations of ionic and nonionic detergents. These are genuine physical alterations, since quite different methods of specimen preservation (negative staining and ice embedding) show parallel effects.

Plasma membranes prepared by mechanical disruption and repeated washing in nonchaotrophic buffers (including sucrose gradients) contained a small population of minimally perturbed gap junctions. These were ordered to varying degrees with lattice dimensions ranging usually between ~86 and 92 Å. Exposure of the plasma membranes to detergents (deoxycholate and Sarkosyl) led to an enrichment of the preparations for gap junctions and a reduction in the center-to-center separation of the connexons (Fig. 2). At the highest detergent concentrations used, the lattice dimensions were as small as 79 Å. Gap junctions isolated by alkali treatment of the plasma membranes had similar lattice dimensions as those of untreated plasma membranes, and showed a parallel contraction of the lattice when exposed to appropriate concentrations of the nonionic detergent, dodecyl maltoside. Moreover, analysis of SDS gel patterns of these specimens demonstrated that no changes in protein composition accompanied detergent treatment, indicating that the observed lattice changes were not due to loss or cleavage of protein.

Analysis of the images revealed that the detergent-induced contraction was accompanied by progressive structural changes. The most striking (Figs. 4, 5) was an increasing deviation from p6m projection symmetry (in which the hexagonal projection of the connexon assemblies is aligned with the unit cell vectors and all (h, k) and (k, h) reflections have equal amplitude and phase). A majority of images of stained junctions with lattice dimensions of 86 Å or greater were within or near experimental error of this symmetry, and increasing deviations were noted as the lattice became smaller. Ice-embedded junctions followed the same pattern, although the agreement with p6m symmetry at large lattice dimensions was not quite as good as in stain, perhaps because of the slightly lower signal-to-noise ratio (and the consequently greater measurement errors; see Table I). Effects due to noise tend to add unidirectionally (downward in Fig. 5 *a* and *b*) because of the consistent handedness imposed on the data. Horizontal and sloping lines drawn in these figures attempt to reduce this unidirectional bias in the data, and probably more closely reflect the true changes in symmetry as a function of lattice dimension.

Interpretation of features in the projection maps must take account of the superposition of densities due to the fact that the gap junction is composed of two layers. Three-dimensional analyses of negatively stained gap junctions (20) have shown that most of the contrast in these images arises from stain deposited in the ~35 Å-wide extracellular gap between the two membranes. Very little contrast arises from stain present at the cytoplasmic-facing surfaces. This partitioning of the contrast simplifies the interpretation of the projection maps from stained specimens. Ice-embedded specimens, on the other hand, provide a view through the entire structure, including the protein within both lipid bilayers (since contrast between protein and lipid is comparable with that between protein and ice), and the superposition in projection is more complicated.

The changes in apparent rotation of the connexon assembly which accompany contraction of the crystal lattice are therefore more easily discussed in relation to the negatively stained specimens. We observed that at large lattice dimensions the densities representing the connexon assembly are aligned approximately parallel to the unit cell directions (Fig. 2 *A*), and that with decreasing lattice dimension they rotate progressively with respect to the lines connecting to their neighbors (Fig. 2 *B*; Figs. 4 and 5). A simple model of connexon–connexon interaction which accounts for these observations is as follows (Fig. 7). At sufficiently large distances between neighbors, the interaction between connexons is due to weak ionic interactions, and the two-dimensional order arises from minimization of energy, with the connexon assemblies free to rotate in the plane of the bilayer. This interaction governs the orientation of the connexon assembly at lattice dimensions of ~86 Å or greater, and favors a rotational orientation in which the connexon assembly and unit cell axes are aligned (Fig. 7 *A*). With addition of detergent, the center-to-center separation of the assemblies decreases, presumably due to depletion of the lipid, and below ~86 Å another set of interactions, either ionic or steric, determines their rotational orientation. As shown in Fig. 7 *B* and *C*, a minimum spacing must be maintained between reference points on each subunit, requiring a twisting of the assemblies with respect to one another and progressively more interlocking as the lattice becomes smaller.

The projection maps of the ice-embedded junctions also support this model of connexon–connexon interaction, displaying the same dependence of apparent rotation of the connexon assembly on lattice dimension. However, the ice-embedded connexon assemblies have their peak positions rotated 30° with respect to those in negative stain. This difference, consistent at both extremes of lattice dimension, may reflect that the subunits are tilted around the central axis (19, 20). Projections dominated by the gap (i.e., images of stained junctions) would then be quite different from those more evenly representing the whole structure (i.e., images of ice-embedded junctions).

That the connexon is indeed able to rotate within the crystal lattice is evident from comparison of three-dimen-

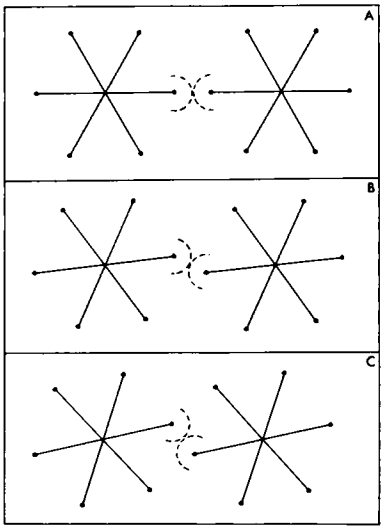

FIGURE 7 Model of the interaction between neighboring connexon assemblies as the lattice becomes smaller. The subunits of each assembly are represented by six radial lines. Semicircular arcs are drawn about reference points located at the ends of neighboring subunits to indicate their distance of closest approach. In *a*, the assemblies are far enough apart (e.g., 88 Å) that they can align with the unit cell axes; in *b*, the assemblies are closer together (e.g., 84 Å apart) and need to rotate (~5°) to maintain a constant distance of closest approach; in *c*, the assemblies are at the minimum distance observed in this study (~80 Å) and need to rotate farther (~12°) to maintain a constant distance of closest approach. The experimental observations are consistent with a scale in which reference points lie at a radius of ~35 Å and the distance of closest approach is ~18 Å.

sional maps obtained from junctions having large lattice dimensions (89 Å [16]) with those having much smaller lattice dimensions (80.6 Å [19]). In the former case the connexons pack almost ridge-against-ridge and in the latter almost ridge-into-groove.

The other systematic effect revealed by the image analysis is an overall strengthening of the six-fold modulations as the lattice contracts (Figs. 2 and 6). These modulations arise from the subunit structure of the connexon, complicated by the superposition which occurs in the paired assembly. In comparing images of junctions with similar lattice dimensions, those in ice are more highly modulated than those in stain. This finding is consistent with three-dimensional analyses (19) which show the subunits to be better resolved in the membrane than in the gap. However, the systematic change in modulation with changing lattice cannot be understood from the projection maps alone, as it could arise from a number of independent factors. One possibility suggested by the three-dimensional studies of gap junctions with large (16) and small (19) unit cell dimensions is that the connexons become differently ordered within the two membrane layers as the connexons come closer together. This may happen because the neighbor-to-neighbor relationships are different in the two layers and there are different constraints on the packing possibilities due to the restricted volume of intervening lipid (19). However other factors, such as varying degrees of rotational disorder of the whole assembly, may also play a significant role.

Previous electron image analyses of negatively stained gap junctions have yielded projection maps similar to those described here, at both extremes of lattice dimension. Images of weakly modulated connexon assemblies organized with approximate p6m projection symmetry were obtained in a low-dose study of gap junctions prepared by treating plasma membranes with sodium deoxycholate (22). These images are similar to those from the junctions with the large lattices. Junctions prepared by other procedures have yielded images which show skewed and more strongly modulated connexon assemblies (1, 2, 7) and which are similar to those from the junctions with the smaller lattices. Thus the difference between the structures described previously can now be understood in light of the lattice-dependent variations reported in this study. Our results also suggest that variability in detergent treatment may be largely responsible for the wide range of lattice dimensions detected by x-ray diffraction (3).

We thank Dr. D.L.D. Caspar for his helpful comments.

This research was supported by a fellowship to Edward Gogol from the Jane Coffin Childs Memorial Fund for Cancer Research, and grants GM27764 and GM30387 to Nigel Unwin from the National Institutes of Health.

Received for publication 18 November 1987 and in final form 21 March 1988.

REFERENCES

1. Baker, T. S., D. L. D. Caspar, C. J. Hollingshead, and D. A. Goodenough. 1983. Gap junction structures. IV. Asymmetric features revealed by low-irradiation microscopy. *J. Cell Biol.* 96:204–216.
2. Baker, T. S., G. E. Sosinsky, D. L. D. Caspar, C. Gall, and D. A. Goodenough. 1985. Gap junction structures. VII. Analysis of connexon images obtained with cationic and anionic negative stains. *J. Mol. Biol.* 184:81–98.
3. Caspar, D. L. D., D. A. Goodenough, L. Makowski, and W. C. Phillips. 1977. Gap junction structures. I. Correlated electron microscopy and x-ray diffraction. *J. Cell Biol.* 74:605–628.
4. Crowther, R. A., and L. A. Amos. 1971. Harmonic analysis of electron microscope images with rotational symmetry. *J. Mol. Biol.* 60:123–130.
5. Furshpan, E. J., and D. D. Potter. 1959. Transmission at the giant motor synapses of the crayfish. *J. Physiol. (Lond.).* 145:289–325.
6. Goodenough, D. A., and W. Stoeckenius. 1972. The isolation of mouse hepatocyte gap junctions. *J. Cell Biol.* 54:646–656.
7. Henderson, D., H. Eibl, and K. Weber. 1979. Structure and biochemistry of mouse hepatic gap junctions. *J. Biol. Chem.* 132:193–218.
8. Hertzberg, E. L. 1984. A detergent-independent procedure for the isolation of gap junctions from rat liver. *J. Biol. Chem.* 259:9936–9943.
9. Hertzberg, E. L., and N. B. Gilula. 1979. Isolation and characterization of gap junctions from rat liver. *J. Mol. Biol.* 254:2138–2147.
10. Kumar, N. L., and N. B. Gilula. 1986. Cloning and characterization

of human and rat liver cDNAs coding for a gap junction protein. *J. Cell Biol.* 103:767–776.

11. Loewenstein, W. R. 1981. Junctional intracellular communication: the cell-to-cell membrane channel. *Physiol. Rev.* 61:829–913.
12. Makowski, L., D. L. D. Caspar, D. A. Goodenough, and W. C. Phillips. 1982. Gap junction structures. III. The effect of variations in the isolation procedure. *Biophys. J.* 37:189–191.
13. Nicholson, B. J., and J-P. Revel. 1983. Gap junctions in liver. Isolation, morphological analysis, and quantitation. *Methods Enzymol.* 98:193–218.
14. Paul, D. L. 1986. Molecular cloning of cDNA for rat liver gap junction. *J. Cell Biol.* 103:123–134.
15. Revel, J-P., B. J. Nicholson, and S. B. Yancey. 1985. Chemistry of gap junctions. *Annu. Rev. Physiol.* 47:263–279.
16. Sikerwar, S., and Unwin, P. N. T. 1988. Three-dimensional structure of gap junctions in fragmented plasma membranes from rat liver. *Biophys. J.* 54:113–119.
17. Subak-Sharpe, H., R. R. Burk, and J. D. Pitts. 1969. Metabolic cooperation between biochemically marked mammalian cells in tissue culture. *J. Cell Sci.* 4:353–367.
18. Unwin, P. N. T., and P. D. Ennis. 1983. Calcium-mediated changes in gap junction structure: evidence from the low angle x-ray pattern. *J. Cell Biol.* 97:1459–1466.
19. Unwin, P. N. T., and P. D. Ennis. 1984. Two configurations of a channel-forming membrane protein. *Nature (Lond.).* 307:609–613.
20. Unwin, P. N. T., and G. Zampighi. 1980. Structure of the junction between communicating cells. *Nature (Lond.).* 283:545–549.
21. Van Oostrum, J., P. R. Smith, M. Mohraz, and R. M. Burnett. 1987. The structure of the adenovirus capsid. III. Hexon packing determined from electron micrographs of capsid fragments. *J. Mol. Biol.* 198:73–89.
22. Warner, A. E., S. C. Guthrie, and N. B. Gilula. 1984. Antibodies to gap-junctional protein selectively disrupt junctional communication in the early amphibian embryo. *Nature (Lond.).* 311:127–131.
23. Zampighi, G., and P. N. T. Unwin. 1979. Two forms of isolated gap junction. *J. Mol. Biol.* 135:451–464.